Fischer-Tropsch Synthesis – investigation of the deactivation of a Co catalyst by exposure to aerosol particles of potassium salt

Ljubiša Gavrilović[a], Jan Brandin[b], Anders Holmen[a], Hilde J. Venvik[a], R. Myrstad[c], Edd A. Blekkan[a,*]

[a] *Norwegian University of Science and Technology, Department of Chemical Engineering, Sem Sælands vei 4, 7491 Trondheim, Norway*

[b] *Linnæus University, Department of Built Environment and Energy Technology, 351 95 Växjö, Sweden*

[c] *SINTEF Materials and Chemistry, NO-7465 Trondheim, Norway*

Abstract

The influence of potassium species on a Co based Fischer-Tropsch catalyst was investigated using an aerosol deposition technique. This way of poisoning the catalyst was chosen to simulate the actual potassium behaviour during the biomass to liquid (BTL) process utilizing gasification followed by fuel synthesis. A reference catalyst was poisoned with three levels of potassium and the samples were characterized and tested for the Fischer-Tropsch reaction under industrially relevant conditions. None of the conventional characterization techniques applied (H_2 Chemisorption, BET, TPR) divulged any difference between poisoned and unpoisoned samples, whereas the activity measurements showed a dramatic drop in activity following potassium deposition. The results are compared to previous results where incipient wetness impregnation was used as the method of potassium deposition. The effect of potassium is quite similar in the two cases, indicating that irrespective of how potassium is introduced it will end up on in the same form and location on the active surface. This indicates that potassium is mobile under FTS conditions, and that potassium species are able to migrate to sites of particular relevance for the FT reaction.

1. Introduction

Population growth and developments in living standards are drivers for increased energy use. Even with the assumption that the world's population will approach steady-state, future energy supplies will be a constraint in world development [1]. High energy cost is forcing scientists and engineers to think about alternative ways of producing fuels, especially transportation fuels which amount to about one quarter of the overall usage of fossil fuels [2]. One alternative option to produce transportation fuels is by the Fischer-Tropsch synthesis (FTS). The main reaction in Fischer-Tropsch synthesis is converting synthesis gas (H_2 + CO) into hydrocarbons (mainly alkanes and alkenes with carbon numbers in the range 1 - 100). Different catalysts can be used in the Fischer-Tropsch synthesis, all based on group 8 metals, such as ruthenium, iron, or cobalt [3]. Ruthenium has a high activity and selectivity, but is regarded as too expensive and rare for industrial application. Cobalt and iron catalysts are the preferred industrial catalysts since they exhibit good combinations of activity, selectivity and stability during the process as well as favourable costs [4]. The main differences in these two catalysts are in their activity and selectivity. Relative to Fe, Co catalysts typically has higher activity as well as selectivity towards higher hydrocarbons (C_{5+}), and lower activity towards the water gas shift (WGS) reaction, thus producing less CO_2 [5]. A lower deactivation rate is also generally found using Co under pure synthesis gas [6], but Co is also more sensitive to impurities. Addition of small amounts of Re or other metals (e.g. Ru, Pt) to the Co based systems mainly enhances catalyst reducibility and increases dispersion [7].

Syngas can be produced from different carbon-containing feedstocks. These feedstocks include coal, natural gas and biomass and the corresponding processes are termed CTL (coal to liquid), GTL (gas to liquid) or BTL (biomass to liquid), respectively. While the CTL and GTL processes are well established, the BTL process has issues regarding the scale and complexity of the process, challenging the economic viability of this route. Different biomass feedstocks are considered, including crop residue, agro-crops, and several tree species [8]. Biomass is a very complex material that besides the C, H and O that dominate the composition contains many other elements that may be undesirable in the syngas due to their potential as catalyst poisons, such as alkali, alkaline earth metal impurities, sulphur and nitrogen. Tar formation during gasification can also be an issue. Potassium is an important nutrient essential for the plant growth and one of the major elements in biomass. In most biomass feedstocks, potassium is the dominant alkali element [9]. The potassium concentration in dry biomass varies between different types of biomass feedstock [10]. For example the K content in a typical dry wood biomass (e.g. spruce and pine sawdust including bark) is reported to be 560ppm [11].

The BTL process involves many steps. After pre-treatment (size reduction, drying), the biomass is fed to the gasifier where the syngas is produced. There are a number of gasifier configurations available, but for the subsequent chemical use of the biomass-based syngas the fluid bed or entrained flow gasifiers are considered as the most suitable [12]. In order to satisfy the requirements of the FTS catalysts, the syngas needs to pass a series of cleaning steps in order to remove contaminants and other undesired species. The syngas must be essentially free of tar, particulates and ash components to prevent catalyst poisoning [13]. The syngas cleaning can be divided into conventional gas cleaning and dry hot gas cleaning. During cooling, alkali species

condense on particulates at 550°C [14]. Consequently, alkali elements can be removed with the particulates by cyclones, filters, scrubbers and packed beds with sorbents at 150-250°C. Alternatively, hot gas cleaning can be considered, where alkali can be removed via chemisorption or physical adsorption at 750 – 900 °C [15], but at present there is no commercially available technology for the high temperature removal of alkali [16].

The requirement (concentration limit) for the alkali species for FT synthesis over cobalt catalysts has been proposed to be below 10ppbv [17]. Although gas cleaning will be employed, poor plant design or operational errors can lead to contamination of the downstream catalysts. Thus, it is important to understand the effect of potential poisons on the FT catalyst. Previously it was shown that alkali species act as poisons, severely deactivating cobalt-based FTS catalysts [18,19]. Cobalt catalysts are known as sensitive to sulphur and some nitrogen compounds, together with alkali and some carbonyl species [6]. Catalyst deactivation by poisoning is often discussed in terms of site blocking, also termed a geometric effect, and electronic effects changing the chemical properties of the surface [20]. Alkali species are electropositively charged, so when deposited on the catalyst surface the charge can be transferred to the surface and influence H_2 and CO adsorption and dissociation [21]. On Fe surfaces this has been attributed to increased adsorption energy of H_2, thereby stabilizing the H_2 molecule and reducing the probability of H_2 dissociation [22]. Blekkan et al. [23] observed rapid desorption of H_2 for K-promoted Co catalyst. The lack of H availability on the Co surface was offered as an explanation for the decrease in activity and increased C_{5+} selectivity. Ma et al. [24] observed increased CO_2 selectivity with increasing potassium loading. This indicates an increase in the WGS activity, which at the outset is low for Co based catalysts.

Previous research in our group [18,19] has been performed using incipient wetness impregnation as a method of deposition of alkali and alkaline earth compounds to Co based catalysts. Although practical, this method differs considerably from the situation in a BTL-plant, where the alkali species are transported to the catalyst surface with the gas phase. In the present work we study the influence of potassium on a Co-based catalyst, introducing aerosol technology as the method for potassium deposition on the Co surface. Potassium nitrate was chosen as a representative salt for this purpose. We aim to show how potassium species in the form of aerosol particles interact with the catalyst, knowledge that can contribute to understanding catalyst deactivation by alkali species. Previous work using this deposition technique showed a decreased conversion of methane in the steam reforming reaction for a Pt/Rh catalyst when exposed to K_2SO_4 aerosol particles compared to the unpoisoned catalyst [25]. As far as we are aware, the technique has not previously been used in relation to cobalt based Fischer-Tropsch synthesis. The results are compared to the previous investigation with the same catalyst and poison, but where incipient wetness impregnation was used as the method of alkali deposition.

2. Experimental

2.1. Catalyst preparation

A 20%Co/0,5%Re/γ-alumina catalyst was used as a reference catalyst during these experiments. A one step incipient wetness impregnation of an aqueous solution of $Co(NO_3)\cdot 6H_2O$ and $HReO_4$ was used as a technique for the catalyst preparation. The support was Puralox γ-alumina from Sasol. After impregnation, the catalyst was dried in a stationary oven (393K, 1h). To improve homogeneity, the sample in a beaker was stirred every 15min. After drying, the catalyst was

calcined in flowing air in a fixed bed quartz reactor at 573K for 16h, using a ramp rate of 2K/min. The final step was sieving the oxidized catalyst precursors to particles size in the range 53-90 microns. The catalyst prepared like this is considered free from impurities, but the support did contain a minor amount of Na (26ppm) [26]. Inductively coupled plasma (ICP-MS) was used to determine ppm levels of potassium.

2.2. Catalyst exposure by aerosol deposition of potassium salts

Potassium nitrate were deposited using the aerosol technology in the apparatus shown in Fig. 1 [25]. KNO_3 dissolved in deionized water (0.025M) was placed in the pneumatic atomizer (Palas GmbH AGK-2000), which produces aerosol particles from the solution. Nitrogen is used as a carrier gas for transporting the generated aerosol particles towards the reactor. On the way, the gas mixture passes an impaction vessel, which separates and traps large particles. In this way a narrow particle size distribution is achieved. The tubular quartz reactor is placed inside an electrically heated oven and the catalyst bed is placed in the middle of the reactor. The lower part of the catalyst bed consists of a glass frit, which allows the gas to pass through, while some aerosols are trapped on the catalyst. A continuous gas flow of 4 l/min was passed through the catalyst bed for three different times on stream; 15min, 60min and 300min. The experiments were performed at 300°C and 1 bar. The drying time of the generated particles at these conditions is in the range of milliseconds, while the residence time of the gas in the oven is in the range of seconds [27].This means that the aerosol particles are completely dry and the salt is transported and deposited in the form of solid particles on the catalyst. Finally the catalyst was calcined ex-situ in air at 573K for 16h.

A scanning mobility particle sizer (SMPS; TSI Inc.) consisting of a differential mobility analyser (DMA; TSI Inc. Model 3081) and a condensation particle counter (CPC; TSI Inc. Model 3010) were used to physically characterize the aerosol particles according to their electrical mobility [25,27]. The SMPS system was used to measure the particle size in the range from ∼20 to 700 nm. A software package with an inversion algorithm is converting the penetration characteristics (aerosol flow of around 0,3l/min) to the particle size distribution. Before entering to the SMPS system, the flow has been dried by a Nafion dryer (Perma Pure Inc., US). To prevent the entrance of larger particles into the system, an impactor device with a cut off size of 805nm was placed right before the SMPS system. The SPMS system has the upper limit of aerosol concentration of 10 000 particles/cm^3. If the concentration of the aerosol particles exceeds this limit, dry compressed air is used to dilute the aerosol flow before entering the SMPS system [28].

Figure 1. *Experimental setup for catalyst exposure to the aerosol particles at 300°C*

2.3. Catalyst characterization

Volumetric adsorption of N_2 was performed on a Tristar II 3020 to determine surface area, pore volume and average pore dimeter of the support materials and prepared catalysts. Before the measurement at liquid nitrogen temperature, the samples (~70mg, particle size 53-90µm) were outgassed in vacuum, first at ambient temperature for 1h and then at 473k overnight. The Brunauer-Emmet-Teller (BET) isotherm [29] was used for calculation of the surface area and the Barret-Joyner-Halenda (BJH) method [30] was applied to determine pore volumes and average pore diameters of the samples.

H_2-chemisorption was performed using a Micromeritics ASAP2010 unit. The catalyst sample (0.2 g) was loaded in the chemisorption reactor. To keep the catalyst in place for the measurement, it was placed between quartz wool wads. Prior to chemisorption, the sample was reduced *in situ*. The sample was heated with a ramping rate of 60 K/h from ambient temperature to 623 K and kept at this temperature in flowing hydrogen for 16 h. The samples were then cooled to 313 K under vacuum. Chemisorption data was collected at 313 K between 0.020 and 0.667 bar H_2 pressure. It was assumed that each surface cobalt atom was one H chemisorption site and that neither Re, alkali impurities or the support contributed to chemisorption.

Temperature programmed reduction (TPR) experiments were performed in an Altamira AMI-300RHP. The catalyst sample (150 mg) was loaded in a quartz u-tube reactor between wads of quartz wool. First the catalyst was treated in flowing inert gas at 200°C and then reduced in hydrogen flow (7% H_2/Ar 50ml/min) to a temperature of 900°C with a ramp rate of 10°C/min. After reaching the final temperature, samples were cooled down to room temperature.

2.4. Fischer–Tropsch synthesis

Fischer–Tropsch synthesis was carried out in four parallel 10 mm ID steel tube fixed bed reactors at 483 K, 20 bar pressure with a H_2/CO ratio of 2.1. A detailed description can be found elsewhere [7]. The samples (1 g) were diluted with inert SiC (20 g) to improve the heat distribution in the bed, and loaded between quartz wool wads to keep the catalyst in place. To further improve heat distribution, aluminium blocks were fixed around the reactors and the reactors were placed in four separate electrically heated furnaces. After leak tests with He, the pressure was kept at 1.5 bar and flowing H_2 was introduced. The temperature was ramped to 623 K (ramp rate 1 K/min),

and kept for 16 h at this temperature. After reduction, the samples were cooled to 443 K. Before introduction of syngas (250 Nml/min) the reactors were pressurized with He to the operating pressure of 20 bar. The temperature program was set to increase the temperature first from 443 to 463 K with a ramp rate of 20 K/min and then to the final temperature of 483 K with a ramping rate of 5 K/min. Liquid Fischer-Tropsch products, i.e. wax and other liquids (water, light hydrocarbons and trace oxygenates), were collected in a hot trap at ~360 K and a cold trap at ambient temperature, respectively. The gas phase was analysed using a HP 6890 gas chromatograph with a GS-Alumina PLOT column, TCD and a flame ionization detector (FID). The synthesis gas contained 3% N_2 which served as an internal standard for quantification of the products to create a mass balance. After ~24 h time on stream (TOS) activity data is reported based on measurements at constant feed rate (250 Nml/min). Then the feed rate of synthesis gas was adjusted to obtain ~50% CO conversion. Selectivity data are reported after ~48 h TOS at 50 ± 5% CO conversion based on the analysis of C_1–C_4 hydrocarbons in gas phase. Since the focus is on the amount of higher hydrocarbons, the selectivity is reported in the usual way as C_5+ and CH_4 selectivity.

3. Results

3.1 Physical characterization of aerosol particles

The generated aerosol particles from potassium nitrate salt have been characterized by SMPS (in the range ~20– 700 nm). The mass size distribution ($\mu g/m^3$) of generated KNO_3 particles is shown in Fig. 2. The obtained average value of particle mass diameter is 206 nm. The mass concentration

(12,7 mg/m^3) is calculated based on the bulk density of KNO_3 (2.1 g/cm^3). All obtained results are presented at normal conditions: 0 °C and 1.01×10^5 Pa taking into account the dilution factor and assuming spherical particles.

Figure 2. *Mass size distribution of KNO_3 aerosol particles*

3.2. Catalyst characterization

Key characterization results are shown in Table 2. The treated samples were compared with the reference catalyst (without impurities). As expected, the untreated sample did not contain potassium, as measured by ICP-MS. For the treated samples, the potassium content increased with increasing exposure time. With respect to chemisorption, there is no significant change among all the samples for any level of potassium. All samples have dispersion around 7.6%, which is the same as the reference catalyst. Regarding catalyst morphological characteristics there is no significant variation; all the samples exhibit similar surface areas (133-137 m^2/g), pore volume (0.47-0.48 cm^3/g) and pore size (~13 nm) within the experimental error for these measurements.

***Table 1*.** Catalysts prepared with the indicated potassium salt impurities and loadings

Temperature programmed reduction profiles of the unpoisoned Co-based catalyst and catalysts poisoned with K are shown in Fig 3. All the samples show a reduction profile typically observed for alumina supported Co catalyst [31]. The two main peaks at ~303°C and ~403°C are assigned to the transition from Co_3O_4 to CoO and CoO to metallic Co, respectively [31]. The small first peak represents the reduction of residual cobalt nitrate [32] remaining from catalyst preparation. The samples containing potassium are showing basically the same TPR profiles as the reference

(potassium free) sample, with the same major peaks for both reduction steps, only marginally shifted to higher temperatures.

Figure 3. *TPR profiles of temperature vs hydrogen consumption of standard catalyst and catalysts with different potassium loadings*

3.3. Fischer-Tropsch Synthesis

The Fischer–Tropsch activity measurements are reported after 24h TOS (time on stream) at a constant feed rate. The catalysts all lose some activity over the first few hours on stream, and the very initial results (first few analyses) are less reliable and are hence not reported. The catalyst activity, reported after 24 h as normalized STY (site time yield) based on H_2 chemisorption, is plotted against potassium impurity loading in Figure 4. Included in Fig. 4 are also results from previous work where K was introduced using IWI (open circles) [19], that are compared to the results from the aerosol-deposited samples prepared in this work (filled circles). Both methods of introducing K result in severe deactivation, and the effect increases with increasing potassium impurity concentration.

Figure 4. *Normalized site time yield (STY) after 24h time on stream (TOS) with different potassium loadings (KNO_3)*

In order to compare Fischer –Tropsch product distribution in a reliable fashion we adjust the conversion to as close to 50% as possible and report the selectivity results obtained after 48h time on stream (TOS). The C_{5+} selectivity is plotted in Figure 5, while CH_4 selectivity is plotted in Figure 6. Again we compare results obtained with the aerosol method used here with results

from catalysts poisoned using the incipient wetness impregnation (IWI). The selectivity for the reference catalyst is determined as 84% and 7,6% for C_{5+} and CH_4, respectively. It can be seen that there is no large influence of potassium on neither the C_{5+} nor the CH_4 selectivity for the aerosol deposition method (filled circles), although the CH_4 shows a weak increasing tendency with increasing potassium amount. This is to some extent in contrast to the results obtained following the IWI method (open circles) [19], which indicates a slight decrease in CH_4 selectivity, and a minor increase in the C_{5+} selectivity with increasing potassium level. But in both cases the effect is small, and we suggest that neither set of data shows any significant change in selectivity towards C_{5+} or CH_4.

The effect of different potassium loadings on CO_2 selectivity is shown in Fig. 7, also reported at 50% CO conversion. In agreement with the our previous work (open circles) as well as Ma et al. [24], the CO_2 selectivity increased slightly with increasing impurity concentration (from 0.15 for the reference catalyst to 0.3 for the catalyst with 400 ppm of K).

Figure 5. *C_{5+} selectivity at 50% of conversion with different potassium loadings (KNO_3)*

Figure 6. *CH_4 selectivity at 50% of conversion with different potassium loadings (KNO_3)*

Figure 7. *CO_2 selectivity at 50% of CO conversion with different potassium loadings (KNO_3)*

4. Discussion

The key observation in this investigation is that the catalysts exposed to potassium using the aerosol deposition technique showed the same behaviour as when potassium was introduced

using incipient wetness impregnation. The most severe effect is on catalyst activity, whereas the effect on characterization results and selectivities in the FTS reaction are insignificant or minute. Importantly, hydrogen chemisorption did not show significant differences between the reference sample and the poisoned catalysts. This is in agreement with the previous work where incipient wetness impregnation was used as the method of deposition, and the dispersion of the Co metal on the catalyst was investigated with different impurities loadings. Lillebø et al. [19] concluded that even a loading of 1000 ppm of alkali metals impurities did not influence the hydrogen chemisorption and Co dispersion.

The important question remaining is where potassium is located after deposition and how it reaches and influences the active sites. As shown in Figure 2, the aerosol particles deposited on the catalyst have dimensions considerably larger (> 100 nm, Fig. 2) than the average pore size of the catalyst (~13 nm,Table 1). This clearly indicates that potassium initially will be deposited on the external surface of the catalyst. The physical characterization does not indicate any blocking of pores or pore openings. The deactivation is significant, however, indicating close contact between potassium and the surface of the supported cobalt nanoparticles during FTS. Larsson et al. [33] studied deactivation of monolithic SCR catalysts using the same technique as applied here, and suggested that the difference observed between aerosol deposition and wet impregnation can be explained by the way of poison penetration into the pore structure. It was proposed that aerosol particles enter the pores by diffusion, possibly resulting in pore mouth blocking. This is valid in the case of diffusion of aerosol particles into the large (geometric) pore structure of the monolith but clearly not the case in our work where the aerosol particles are much larger than the average pore size and have no effect on the measured physical parameters

of the catalyst. In contrast is the penetration process during impregnation driven by capillary forces, where the solution fills the complete pore structure including meso- and micropores. Thus, after impregnation is the potassium salt located close to or on the cobalt particles. However, neither poisoning method results in any change in the characterization features, and both give similar, significant losses in activity per amount of potassium added. Hence at the point when the activity results are recorded, (24 h TOS) it seems that the location of all or some of the potassium is the same in the two cases. This must be attributed to potassium mobility, most probably at reaction conditions. One mechanism explaining this could be that potassium is transported as volatile species. After aerosol deposition and subsequent calcination are the aerosol particles probably still in the form of potassium nitrate KNO_3, which exhibits considerable thermal stability. But under FT reaction conditions, at relatively high temperatures, and in the presence of a significant H_2O partial pressure and syngas, the formation of mobile potassium species is possible. This way potassium can be transported to sites where it has the observed effect on the catalytic activity. This implies that at least some of the potassium is located on the cobalt particles.

It has been suggested that potassium simply block the active sites, e.g. corner and low coordination edge sites active in H_2 dissociation thus blocking catalytic activity [6]. Alternatively, it has been proposed that the alkali metal is promoting CO dissociation by acting as an oxygen acceptor, decreasing the number of available sites for H_2 dissociation [34]. The alkali metal may also decrease the rate of H_2 dissociation by back-donation of electrons to the Co surface, since dissociative adsorption of H_2 induces electron donation to the metal surface [35]. This was however proposed based on dosing the catalysts with rather high amounts of Na (Na/Co ratio

was 0.69, Na loading 7 wt%), which is a much higher concentration than the low amounts of K used here. In this case the influence on the chemisorption properties was clear, as evidenced in the reported IR spectra of adsorbed CO. Combined experimental and theoretical Co model system (Co(11-20) investigations in our group indicated step edges as the preferred location of deposited, metallic K. The presence of K on the Co surface also inhibited the CO-induced surface reconstruction, which might explain loss of activity under FT reaction [36].

Recently we have also used density functional theory (DFT) to investigate the potassium interaction with cobalt surfaces (Q. Chen et al. [37]). The DFT calculation gave similar adsorption energies for K on different high symmetry sites on many of the Co surfaces, including the B5-type sites often suggested (see e.g. [38]) to be active sites in the FTS reaction. The diffusion barriers for K on cobalt surfaces are very low, implying that K is mobile once located on a cobalt particle. In another word K atoms might have a tendency towards occupying the most favourable adsorption sites (e.g. B5, B6 sites), which also could be the important sites for the FT reaction. Since during FT synthesis many species will be absorbed on the Co surface such as CO*, H*, HCO*, etc. [39] it is important to take into account the influence of these adsorbates on K mobility. The mobility of K and Co on Ru (001) surface was investigated using a laser-induced thermal desorption (LITD) techniques. Diffusion results for potassium in the presence of CO implied that potassium diffusion is severely hindered when $\theta_{CO}>\theta_K$ [40]. Westre et al. [41] used a laser-induced thermal desorption (LITD) technique to investigate the surface diffusion of potassium on Ru(001). The potassium surface mobility changed dramatically with changes in K coverage. The surface diffusion coefficient was doubled when potassium coverage increased from 0.08 to 0.33 ML. When the surface diffusion coefficient increases as a function of increasing coverage it usually

indicates the repulsive lateral interactions between adsorbates. Vaari et al. [42] investigated the repulsive interaction between potassium atoms on clean Co (0001), where the potassium desorption peak is visible at 430°C. This repulsive interaction between potassium atoms might be the reason why it is still possible to chemisorb hydrogen on Co surface when K is present on the surface.

Our results are best explained by taking into account the mobility of potassium. We speculate that the redistribution of K occurs rapidly during early stages of FTS. This will be during the initial transient period of the experiment, thus very difficult to observe. A consequence of this idea is that ex-situ characterization (e.g. H_2 chemisorption) in this case is less representative of the working catalyst. Our findings could also have implications for the understanding of the FTS mechanism, for which several mechanistic options are available [43]. The proposed mechanisms differ in the formation and identity of the building monomer and how this monomer is adding to the growing hydrocarbon chain. It is very important to understand the propagation mechanism since it can govern the hydrocarbon selectivity [44]. Potassium species might affect or even change pathways in the mechanism during FT synthesis. Further theoretical work as well as improved experimental procedures are needed in order to be able to understand K influence on different transitions states in the FT mechanism.

5. Conclusion

The purpose of this investigation is a better understanding of the alkali influence on Co-based F-T catalyst and issues relevant to the conversion of biomass to liquid fuels via gasification. We have adapted a technique to transfer potassium species in the form of aerosols to the Co catalyst

surface. This new approach can better simulate the behaviour during the real industrial process, thus provide simulation of *in situ* poisoning and therefore give a more realistic picture of the effect of potassium. Samples poisoned by aerosol deposition were tested and compared with the results where an incipient wetness impregnation technique was used as a method of deposition. Results of this work provide further evidence that potassium acts as a strong poison. Catalyst activity was reduced by about 25% with only 400 ppm potassium, which is very close to the results obtained with impregnation of the potassium salt. The similarity in behaviour indicates that potassium ends up in the same form and location on the surface, with a very small amount having a profound effect on the catalyst activity. This is in agreement with the idea that potassium is mobile under FTS conditions, and that potassium species tend to can migrate towards FTS active sites.

Acknowledgements

Project name: Advanced Biofuels via Synthesis Gas; Financial support: The Research council of Norway, ENERGIX programme (contract no: 10417501).

References

[1] J.P. DeLong, O. Burger, M.J. Hamilton, S. Collins, A. Dobson, PLoS One (2010). *http://doi.org/101371/journal.pone.0013206*.

[2] J.P. Lange, Biofuels, Bioprod. Biorefining 1 (2007) 39–48.

[3] M. Vannice, J. Catal. 37 (1975) 449–461.

[4] A.Y. Khodakov, W. Chu, P. Fongarland, Chem. Rev. 107 (2007) 1692–744.

[5] R. Luque, A.R. de la Osa, J.M. Campelo, A.A. Romero, J.L. Valverde, P. Sanchez, Energy Environ. Sci. 5 (2012) 5186.

[6] N.E. Tsakoumis, M. Rønning, Ø. Borg, E. Rytter, A. Holmen, Catal. Today 154 (2010) pp. 162–182.

[7] Ø. Borg, N. Hammer, S. Eri, O.A. Lindvåg, R. Myrstad, E.A. Blekkan, M. Rønning, E. Rytter, A. Holmen, Catal. Today 142 (2009) 70–77.

[8] S.S. Ail, S. Dasappa, Renew. Sustain. Energy Rev. 58 (2016) 267–286.

[9] M.P. Glazer, N.A. Khan, W. de Jong, H. Spliethoff, H. Schurmann, P. Monkhouse, Energy & Fuels 19 (2005) 1889–1897.

[10] L.L. Baxter, T.R. Miles, T.R. Miles, B.M. Jenkins, T. Milne, D. Dayton, R.W. Bryers, L.L. Oden, Fuel Process. Technol. 54 (1998) 47–78.

[11] K. Froment, F. Defoort, C. Bertrand, J.M. Seiler, J. Berjonneau, J. Poirier, Fuel 107 (2013) 269–281.

[12] V.S. Sikarwar, M. Zhao, P.S. Fennell, N. Shah, E.J. Anthony, Prog. Energy Combust. Sci. 61 (2017) 189–248.

[13] H. Leibold, A. Hornung, H. Seifert, Powder Technol. 180 (2008) 265–270.

[14] K. Göransson, U. Söderlind, J. He, W. Zhang, Renew. Sustain. Energy Rev. 15 (2011) 482–492.

[15] C.N. Hamelinck, A.P.C. Faaij, J. Power Sources 111 (2002) 1–22.

[16] M.J.A. Tijmensen, A.P.C. Faaij, C.N. Hamelinck, M.R.M. Van Hardeveld, Biomass and Bioenergy 23 (2002) 129–152.

[17] H. Boerrigter, H.P. Calis, D.J. Slor, H. Bodenstaff, 2nd World Conf. Technol. Exhib. Biomass Energy, Ind. Clim. Prot. (2004) 10–14.

[18] C.M. Balonek, A.H. Lillebø, S. Rane, E. Rytter, L.D. Schmidt, A. Holmen, Catal. Letters 138 (2010) 8–13.

[19] A.H. Lillebø, E. Patanou, J. Yang, E.A. Blekkan, A. Holmen, Catal. Today 215 (2013) pp. 60–66.

[20] H.P. Bonzel, G. Brodén, H.J. Krebs, Appl. Surf. Sci. 16 (1983) 373–394.

[21] F. Solymosi, I. Kovacs, J. Phys. Chem. 93 (1989) 7537–7539.

[22] G. Ertl, S.B. Lee, M. Weiss, Surf. Sci. 111 (1981) L711–L715.

[23] E.A. Blekkan, A. Holmen, S. Vada, Acta Chem. Scand. 47 (1993) 275–280.

[24] W.P. Ma, Y.J. Ding, L.W. Lin, Ind. Eng. Chem. Res. 43 (2004) 2391–2398.

[25] J. Einvall, S. Albertazzi, C. Hulteberg, A. Malik, F. Basile, A.C. Larsson, J. Brandin, M. Sanati, Energy and Fuels 21 (2007) 2481–2488.

[26] Ø. Borg, S. Eri, E.A. Blekkan, S. Storsæter, H. Wigum, E. Rytter, A. Holmen, J. Catal. 248 (2007) 89–100.

[27] W.C. Hinds, Aerosol Technology: Properties, Behavior, and Measurement of Airborne Particles, John Wiley & Sons, 2012.

[28] F. Moradi, J. Brandin, M. Sohrabi, M. Faghihi, M. Sanati, Appl. Catal. B Environ. 46 (2003) 65–76.

[29] S. Brunauer, P.H. Emmett, E. Teller, J. Am. Chem. Soc. 60 (1938) 309–319.

[30] E.P. Barrett, L.G. Joyner, P.P. Halenda, J. Am. Chem. Soc. 73 (1951) 373–380.

[31] M. Rønning, N.E. Tsakoumis, A. Voronov, R.E. Johnsen, P. Norby, W. Van Beek, Ø. Borg, E. Rytter, A. Holmen, Catal. Today 155 (2010) 289–295.

[32] A. Bao, J. Li, Y. Zhang, J. Nat. Gas Chem. 19 (2010) 622–627.

[33] A.C. Larsson, J. Einvall, A. Andersson, M. Sanati, Top. Catal. (2007) pp. 149–152.

[34] B.C. Enger, A. Holmen, Catal. Rev. 54 (2012) 437–488.

[35] C. Mirodatos, E. Brum Pereira, A. Gomez Cobo, J.A. Dalmon, G.A. Martin, Top. Catal. 2 (1995) 183–192.

[36] M.D. Strømsheim,.I.H. Svenum,.M.H. Farstad, Z. Li, L. Gavrilovic, X. Guo, S. Lervold, A. Borg, H.J. Venvik, Catal. Today (2016). https://doi.org/10.1016/j.cattod.2017.05.086

[37] Q. Chen, I. Svenum, Y. Qi, L. Gavrilovic, D. Chen, A. Holmen, E.A. Blekkan, E. Rytter, U.M. Graham, G.A. Thomas, B.H. Davis, Phys. Chem. Chem. Phys. 92 (2017) 17–24.

[38] J. Cheng, P. Hu, P. Ellis, S. French, G. Kelly, C.M. Lok, J. Phys. Chem. C 114 (2010) 1085–1093.

[39] J. Yang, Y. Qi, J. Zhu, Y.A. Zhu, D. Chen, A. Holmen, J. Catal. 308 (2013) 37–49.

[40] E.D. Westre, D.E. Brown, J. Kutzner, S.M. George, J. Chem. Phys. 104 (1996) 7313–7324.

[41] E.D. Westre, D.E. Brown, J. Kutzner, S.M. George, Surf. Sci. 294 (1993) 185–196.

[42] J. Vaari, J. Lahtinen, P. Hautojarvi, Catal. Lett. 44 (1997) 43–49.

[43] R. A. van Santen, A. J. Markvoort, I. A. W. Filot, M.M. Ghouri, E.J.M. Hensen, Phys. Chem. Chem. Phys. 15 (2013) 17038–63.

[44] Y. Qi, J. Yang, D. Chen, A. Holmen, Catal. Letters 145 (2015) 145–161.

Table 1. Catalysts prepared with the indicated potassium salt impurities and loadings

Potassium salt impurity	Potassium amount (ppm)	Dispersion (%)	Bet surface area (m^2/g)	Pore volume (cm^3/g)	Pore size (nm)	Reduction temperature (°C)	
						$Co_3O_4 \rightarrow CoO$	$CoO \rightarrow Co$
None	None	7,6	133	0,47	13,1	295	403
KNO3	26	7,4	137	0,48	13,3	300	403
KNO3	96	8,1	135	0,48	13,3	311	423
KNO3	379	7,5	136	0,48	13,1	304	406

Captions for figures

Figure 1. *Experimental setup for catalyst exposure to the aerosol particles at 300°C*

Figure 2. *Mass size distribution of KNO_3 aerosol particles*

Figure 3. *TPR profiles of temperature vs hydrogen consumption of standard catalyst and catalysts with different potassium loadings*

Figure 4. *Normalized site time yield (STY) after 24h time on stream (TOS) with different potassium loadings (KNO_3)*

Figure 5. *C5+ selectivity at 50% of conversion with different potassium loadings (KNO_3)*

Figure 6. *CH_4 selectivity at 50% of conversion with different potassium loadings (KNO_3)*

Figure 7. *CO_2 selectivity at 50% of CO conversion with different potassium loadings (KNO_3)*

Figure 1.

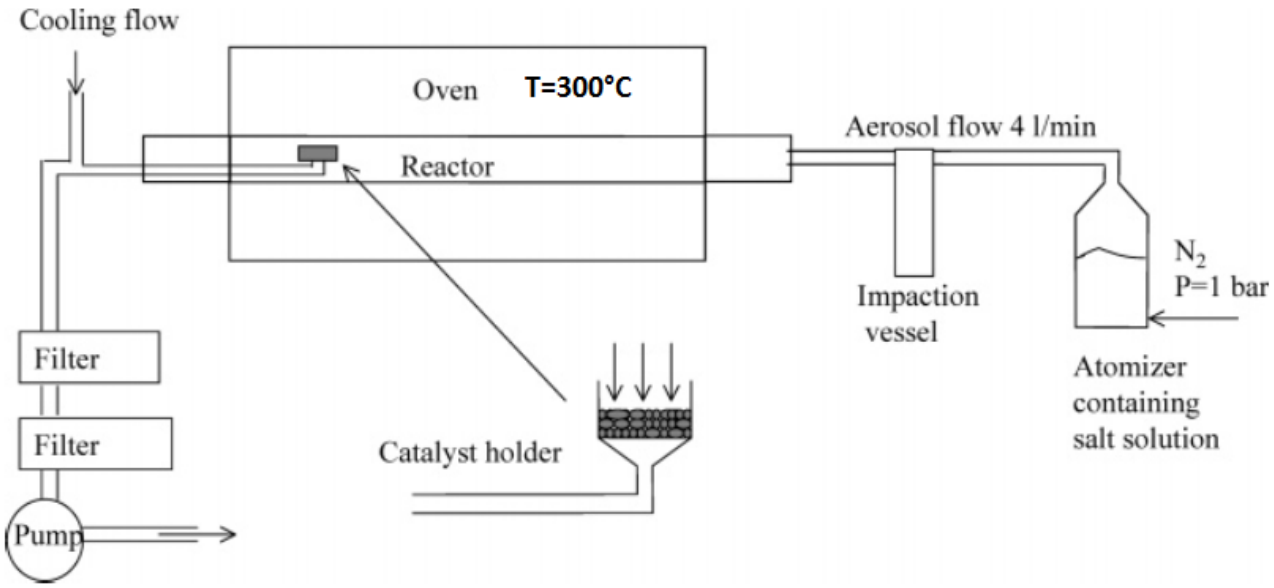
Cooling flow
Oven
T=300°C
Reactor
Aerosol flow 4 l/min
Impaction vessel
N_2
P=1 bar
Atomizer containing salt solution
Filter
Filter
Pump
Catalyst holder

Figure 2.

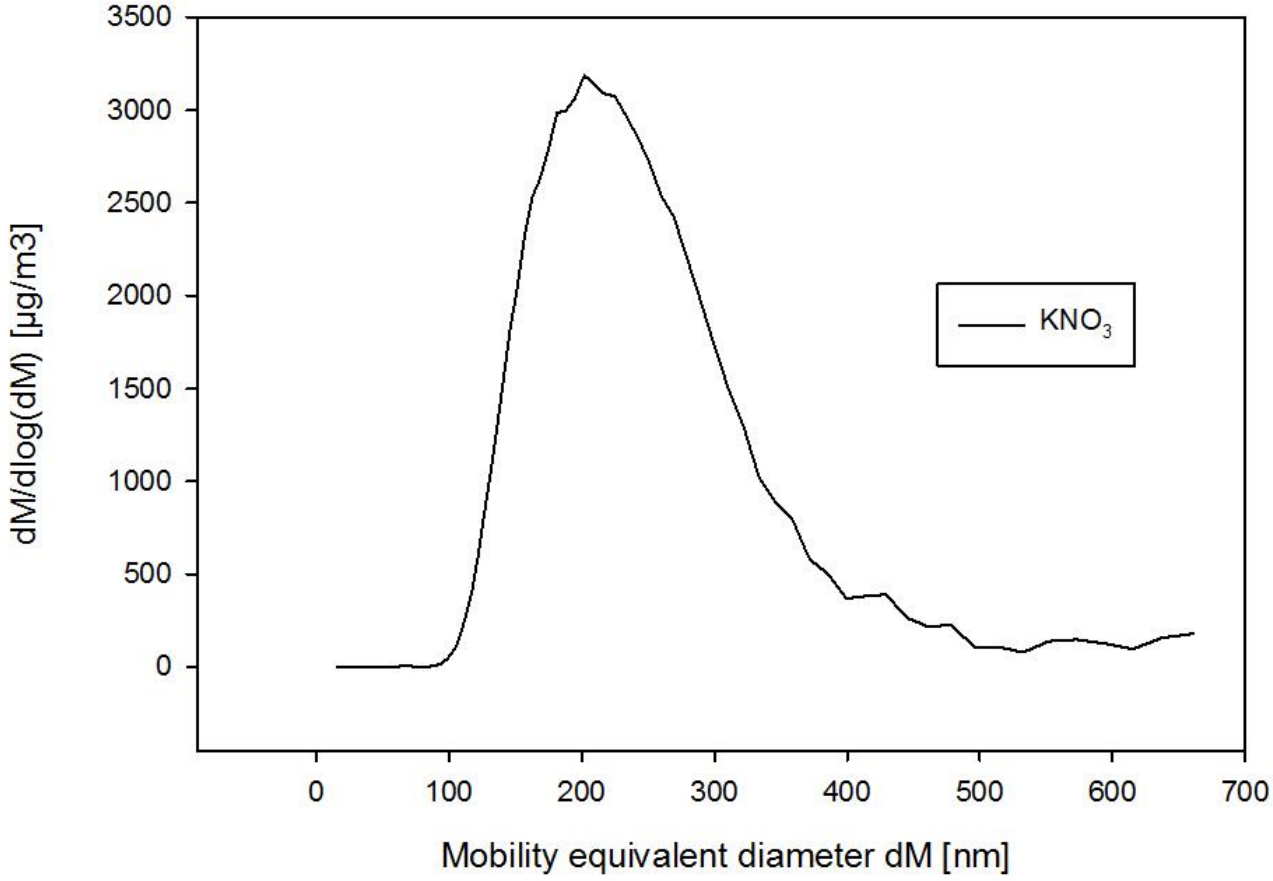
3500
3000
2500
2000
1500
1000
500
0
dM/dlog(dM) [µg/m3]
KNO3
0
100
200
300
400
500
600
700
Mobility equivalent diameter dM [nm]

Figure 3.

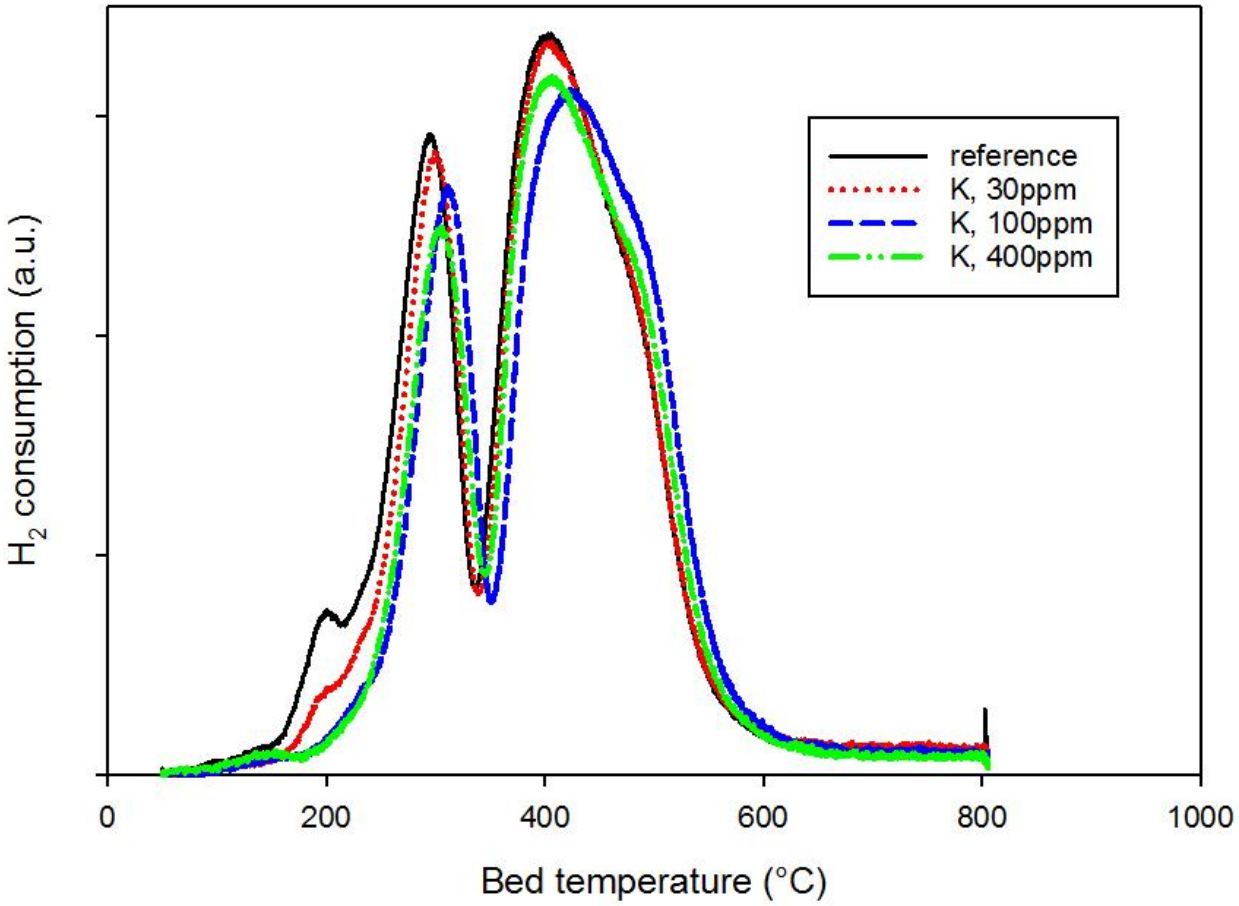
reference
K, 30ppm
K, 100ppm
K, 400ppm
H2 consumption (a.u.)
0
200
400
600
800
1000
Bed temperature (°C)

Figure 4.

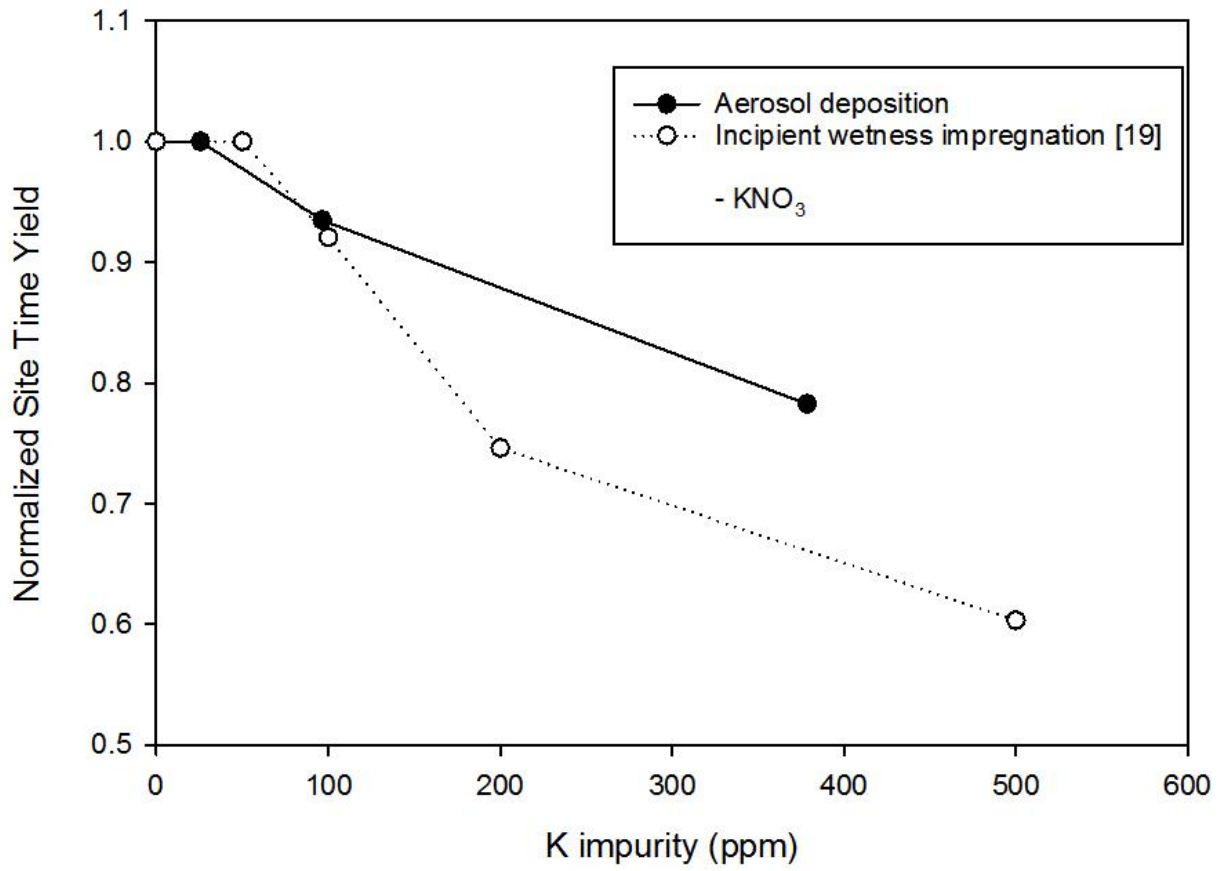
Aerosol deposition
Incipient wetness impregnation [19]
- KNO3
Normalized Site Time Yield
K impurity (ppm)
1.1
1.0
0.9
0.8
0.7
0.6
0.5
0
100
200
300
400
500
600

Figure 5.

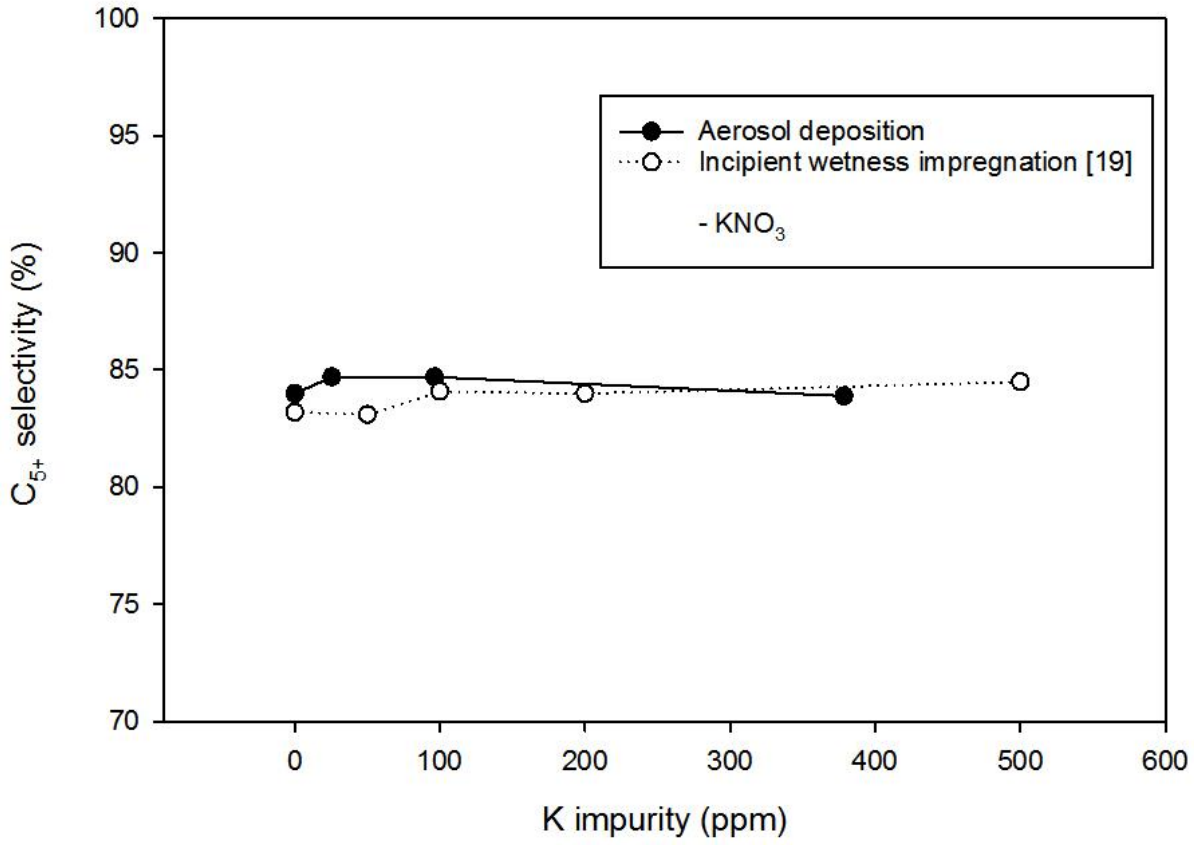
100
95
90
85
80
75
70
C_{5+} selectivity (%)
0
100
200
300
400
500
600
K impurity (ppm)
Aerosol deposition
Incipient wetness impregnation [19]
- KNO_3

Figure 6.

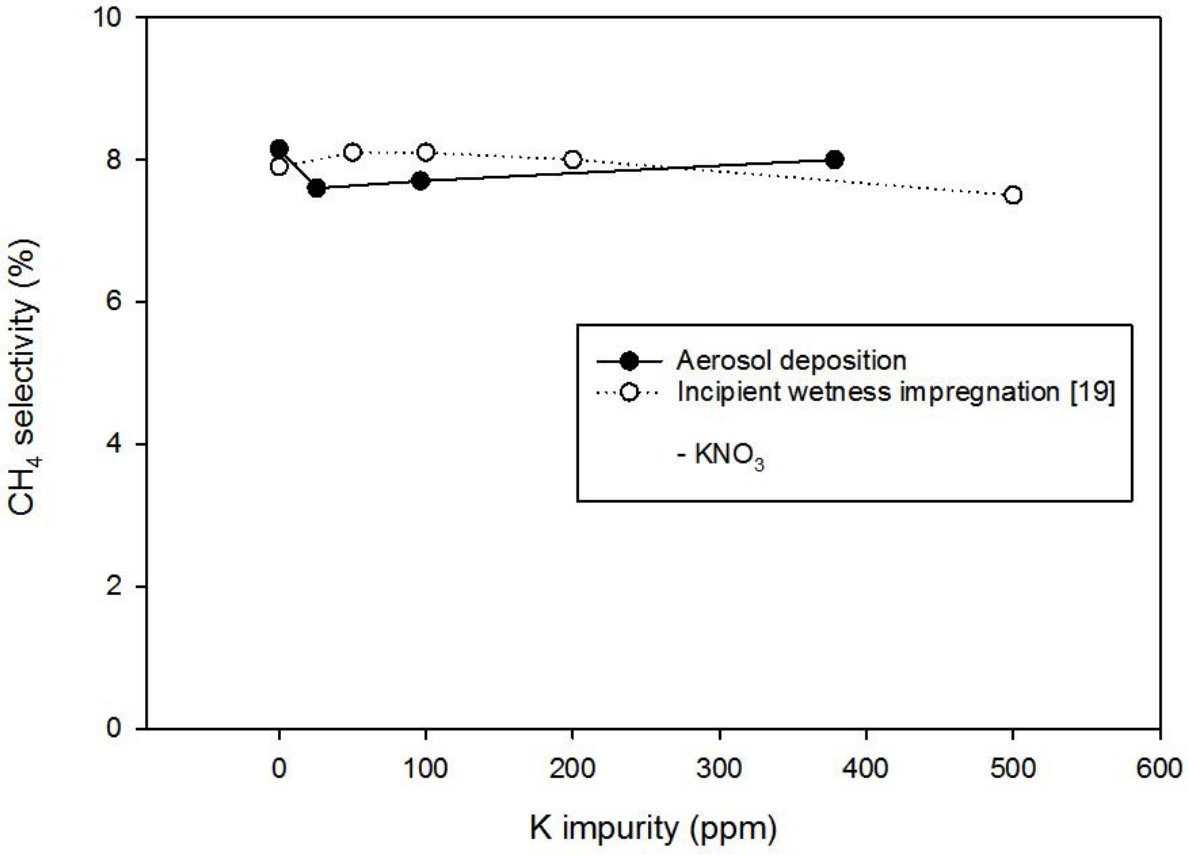
10
8
6
4
2
0
CH_4 selectivity (%)
0
100
200
300
400
500
600
K impurity (ppm)
Aerosol deposition
Incipient wetness impregnation [19]
- KNO_3

Figure 7.

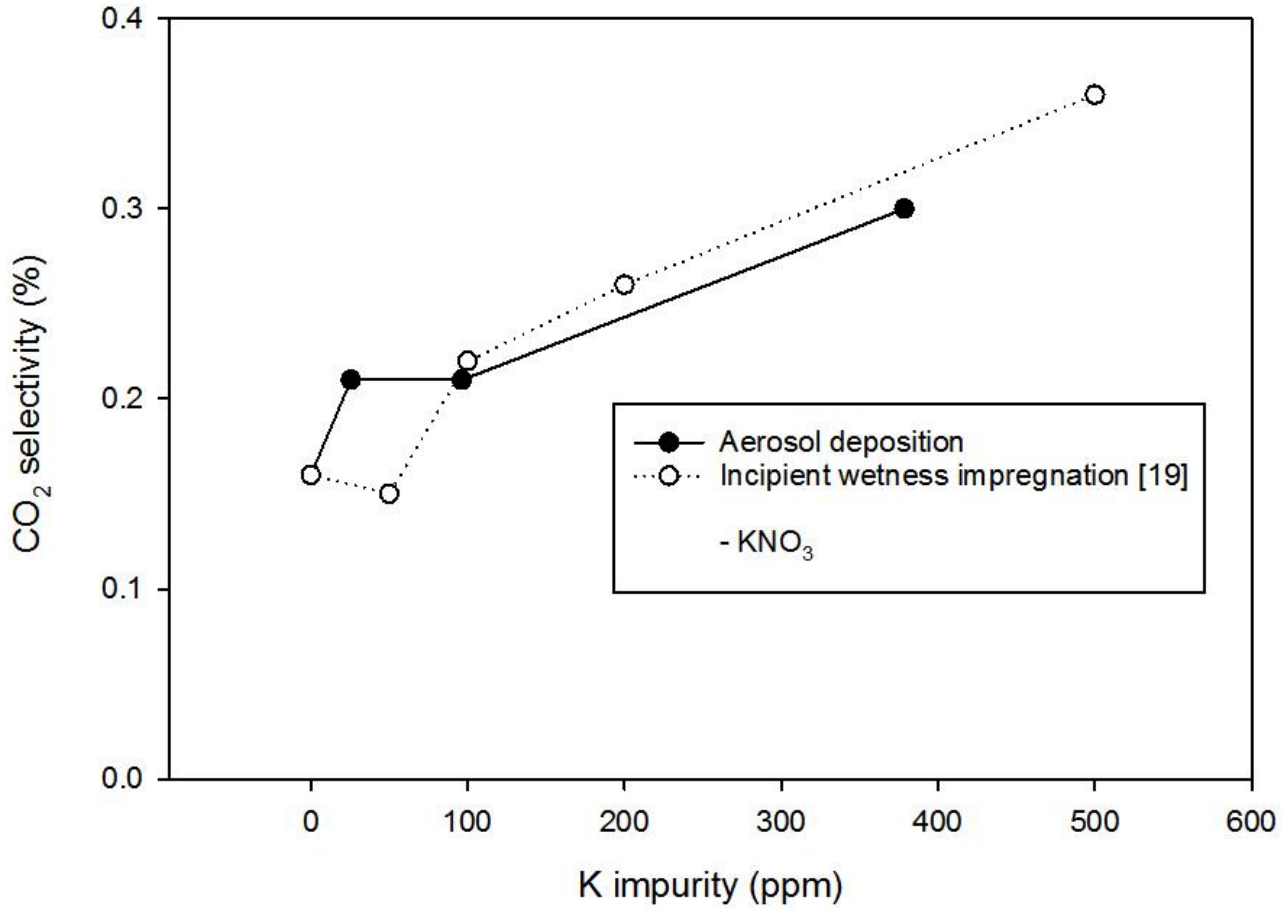
0.4
0.3
0.2
0.1
0.0
CO_2 selectivity (%)
0
100
200
300
400
500
600
K impurity (ppm)
Aerosol deposition
Incipient wetness impregnation [19]
- KNO_3